Carbon dioxide dissociation in a microwave plasma reactor operating in a wide pressure range and different gas inlet configurations

Carbon Dioxide Dissociation in a Microwave Plasma Reactor operating in a wide pressure range and different gas inlet configurations

Igor Belov*, Vincent Vermeiren, Sabine Paulussen and Annemie Bogaerts

---

I. Belov, Dr. S. Paulussen

Sustainable Materials Management, VITO, Boeretang 200, 2400 Mol, Belgium

E-mail: igor.belov@vito.be, sabine.paulussen@vito.be

I. Belov, V. Vermeiren, Prof. Dr. A Bogaerts

PLASMANT, Department of Chemistry, University of Antwerp, B-2610 Wilrijk-Antwerp, Belgium

E-mail: Vincent.Vermeiren@uantwerpen.be. annemie.bogaerts@uantwerpen.be

---

Keywords: conversion; plasma; Microwave; discharge;

Abstract

Microwave (MW) plasmas represent a promising solution for efficient CO_2 dissociation. MW discharges are also very versatile and can be sustained at various pressure and gas flow regimes. . To identify the most favorable conditions for the further scale-up of the CO_2 decomposition reaction, a MW plasma reactor operating in pure CO_2 in a wide pressure range (200 mbar - 1 bar) is studied. Three different gas flow configurations are explored: a direct, reverse and a vortex regime. The CO_2 conversion and energy efficiency drop almost linearly with increasing pressure, regardless of the gas flow regime. The results obtained in the direct flow configuration underline the importance of post-discharge cooling, as the exhaust of the

MW plasma reactor in this regime expanded into the vacuum chamber without additional quenching. As a result, this system yields exhaust temperatures of up to 1000 K, which explains the lowest conversion (~3.5% at 200 mbar and 2% at 1 bar). A post-discharge cooling step is introduced for the reverse gas inlet regime and allows the highest conversion to be achieved (~38% at 200 mbar and 6.2% at 1 bar, with energy efficiencies of 23% and 3.7%). Finally, a tangential gas inlet is utilized in the vortex configuration to generate a swirl flow pattern. This results in the generation of a stable discharge in a broader range of CO_2 flows (15-30 SLM) and the highest energy efficiencies obtained in this study (~25% at 300 mbar and ~13% at 1 bar, at conversions of 21% and 12%). The experimental results are complemented with computational fluid dynamics simulations and with the analysis of the latest literature to identify the further research directions.

1 Introduction

The global need for efficient CO_2 utilization technologies recently highlighted new ideas for re-use and conversion of CO_2 waste streams into added-value products [1-5]. Multiple papers demonstrated the potential of different plasma systems for activation and dissociation of this highly inert gas [6-16]. In general, microwave (MW) discharges are considered to be one of the most promising plasma systems for CO_2 decomposition due to their capability to utilize the highly efficient vibrational excitation kinetics of the non-equilibrium discharge [10, 17-19]. In this way, it is possible to realize CO_2 dissociation with a higher energy efficiency than in the conventional thermal process [5, 20]. From a technological point of view, MW plasma systems represent an electrodeless solution with a high electric energy utilization efficiency and a fast switching on time [21]. Another advantage of CO_2 decomposition in a MW discharge reactor relates to the possibility to utilize electricity produced from renewable sources, thus balancing the power grid [3].

Historically the most successful experiments on CO_2 conversion in a MW discharge were performed in the 1980s in the USSR [20, 22]. Energy efficiencies up to 90% were achieved when a supersonic flow regime was utilized at reduced pressure of about 200 mbar. The topic was brought up again more recently in response to the spread of intermittent renewable electricity sources and the general acceptance of the need to fight global warming. Attempts to reproduce the conditions and results reported in the work of Fridman *et al.* have been made, but energy efficiencies only up to 51% were demonstrated so far in this case [23]. Besides that, a lot of novel approaches to improve the performance of CO_2 decomposition in MW plasma systems were recently presented. Chen *et al.* reported a twofold increase of the conversion and energy efficiency when a NiO catalyst on a TiO_2 support was installed downstream of a surface-wave MW CO_2 discharge [24-26], reaching a conversion and energy efficiency of both 42%. Uhm *et al.* reported a high CO_2 conversion (45%, but with an energy efficiency of only 8%) for an atmospheric pressure MW plasma torch with a post-discharge coal powder gasification system [27]. Mitsingas *et al.* presented a highly efficient CO_2 dissociation process in a compact atmospheric pressure MW plasma reactor [28], achieving 50-80% energy efficiency, but at low conversion (9-3%). The introduction of gas admixtures to a CO_2 MW discharge could be used to achieve some degree of control over the plasma parameters and to utilize more efficient pathways for CO_2 decomposition. The influence of Ar [29, 30], N_2 [31], H_2 [32, 33] and H_2O [24-26, 34] gas admixtures on CO_2 dissociation in a MW plasma was demonstrated experimentally and by modeling. Such research is also important for the future up-scaling of the process, as gas impurities are inevitable on an industrial scale.

Another ongoing research direction related to efficient CO_2 decomposition in a MW plasma is targeting *in-situ* diagnostics to allow a better understanding of the discharge mechanisms and process control [23, 29, 30, 35, 36]. Likewise, modeling has also proven to

give valuable insight in the underlying mechanisms of CO_2 dissociation in a MW plasma, including the role of vibrational kinetics, and identifying the limitations in the conversion and energy efficiency in a wide range of conditions [17-19, 31].

Despite all the recent attention to this technology, studies of the MW plasma operating in CO_2 in a broad range of process parameters and gas flow configurations are still rare. Usually only a very limited parameter range is presented. Moreover, given the development stage of the technology, it is still unclear which discharge conditions are the most beneficial for scale-up. In this paper, we utilize the opportunity to generate a stable MW discharge in pure CO_2 over a wide pressure range and with different gas inlet regimes to study the CO_2 conversion reaction in this broad range of conditions. Thus, the aim of this paper is to demonstrate the influence of pressure, gas flow configuration and post-discharge cooling on the CO_2 decomposition process in a MW discharge reactor. This work will be useful for further up-scaling of MW plasma systems, which will be necessary to bring plasma-based CO_2 conversion into real application.

2 Experimental

The experiments are performed in a MW plasma system composed of the commercial IPLAS *CYRANNUS* plasma source mounted on top of a stainless steel vacuum chamber (cf. **Figure 1**). The principle of this MW plasma source is based on a resonator with annular slot antennas [37]. This special set-up allows to sustain a MW discharge in a very wide pressure range, from low (10^{-2} mbar) to atmospheric pressure (1 bar).

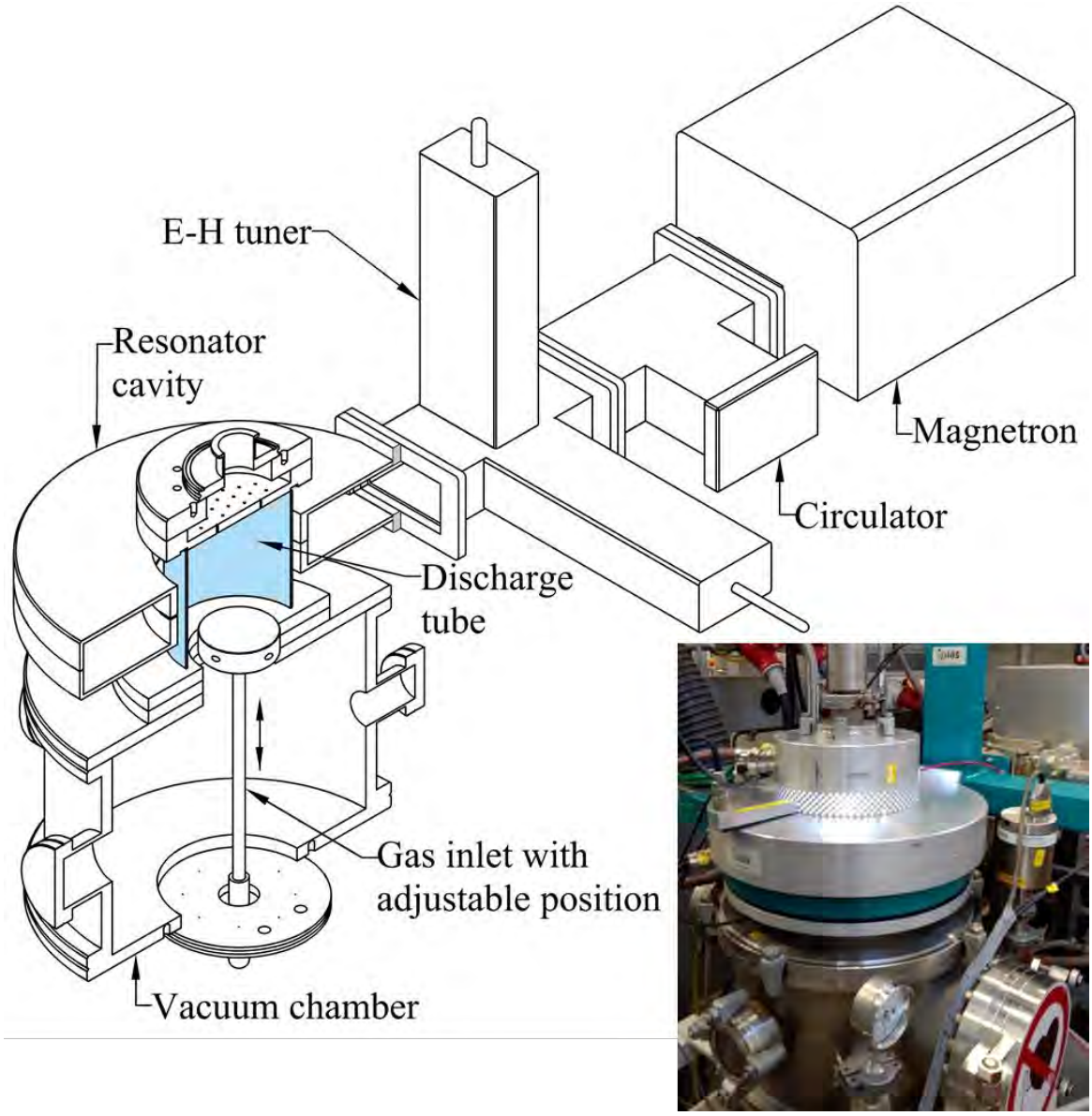

Figure 1. Drawing and picture of the MW discharge system. The MW discharge tube is indicated with pale blue colour in the schematic drawing.

2.1 Microwave system

The 2.45 GHz magnetron supply with a maximum output of 6 kW microwave field is connected through a circulator and an E-H tuner to the resonator cavity. The plasma is formed in a cylindrical quartz tube with a diameter of 140 mm and a height of 140 mm, which corresponds to a volume of 2.1 liters. The discharge tube is connected via a DN350

flange to a chamber with a height of 235 mm and overall volume of 22 liters. The reflected power is measured via the microwave detector installed in the circulator and minimized by the E-H tuner, which is used as an impedance matching device. The circulator, magnetron and the plasma-exposed parts of the discharge cell are all water-cooled, while the resonator and the outer surface of the quartz tube are air-cooled.

2.2 Gas supply and vacuum scheme

The gas supply and vacuum systems are shown in **Figure 2**. Prior to operation, the vacuum chamber is pumped down to 20 mbar via a rotary and Roots pump installed in series. The pressure is set via a control valve and a pressure gauge, while CO_2 flow is supplied through a mass flow controller (MFC). With 2-6 kW MW power input the discharge can be ignited without an additional inert gas admixture or electric field concentrator at a maximum pressure of about 100 mbar when 5-30 SLM CO_2 is supplied to the system. After the breakdown, the pressure in the chamber can be further increased up to 1 bar, while the plasma remains to be sustained.

CO_2 dissociation is taking place in the plasma according to reaction 1:

$$CO_2 \rightarrow CO + 0.5\,O_2, \quad \Delta H = 2.9\ eV / molecule \tag{1}$$

To evaluate the CO_2 conversion and corresponding energy efficiency in the MW discharge, the gas mixture is sampled from the exhaust pipe to the gas chromatograph (GC) through a diaphragm pump. The formulas below are used to calculate the CO_2 conversion (Equation 2**)**, specific energy input (SEI, Equation 3) and energy efficiency of the process[38] (Equation 4**)**:

$$\mathrm{CO_2\ Conversion\ (\%)} = [1 - \frac{moles\ CO_{2,\ Plasma\ \ ON}}{moles\ CO_{2,\ Plasma\ \ OFF}}] \times 100\% \quad (2)$$

$$\mathrm{SEI\ (eV/molec.)} = \frac{P_{Input}(W) \cdot 60(\mathrm{sec/\ min})}{Flow\ rate(ml/\mathrm{min}) \cdot 3.92(eV \cdot ml/J \cdot molec.)} \quad (3)$$

$$\mathrm{Energy\ efficiency\ (\%)} = \mathrm{CO_2\ Conversion(\%)} \cdot \frac{\Delta H(\mathrm{eV/molec.})}{SEI(\mathrm{eV/molec.})} \quad (4)$$

We use the input power in equation 3, and not the plasma power as is often done in the literature [23, 26, 32, 35]. In some systems, like DBDs, the plasma power can be only half of the input power, but in the MW system, the difference is usually quite small (can be estimated to be around 10% [21]). Still, there are some losses due to the reflectance of the incident MW (that is minimized but still present) and unwanted absorbance on the discharge parts. Note that if we would use the plasma power in our calculation, the reported energy efficiencies (see below) would be ca. 5-10% higher. In our case the power provided by the power supply was used as input power, however to estimate the plasma power, the reflected power should be subtracted. It can be done by measuring the reflected power, for instance by the calibrated MW power detector connected to the isolator or by means of calorimetry.

It is known that the gas expansion due to the chemical reaction of CO_2 decomposition (Reaction 1) can lead to a faulty CO_2 conversion estimation [31, 39]. In our system, however, the pressure regulation and exhaust sampling to the GC by the diaphragm pump (that provides constant pressure and flow rate at the point of injection to the GC), allow us to consider this effect to be negligible.

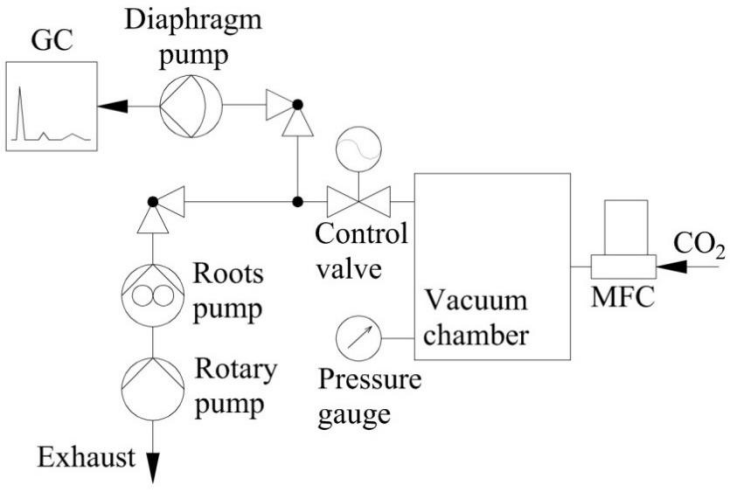

Figure 2. Gas supply and vacuum scheme of the MW set-up used.

2.3 Design of the gas inlet configurations

The way the gas is supplied to the reactor has a significant influence on the MW discharge operation [21]. In this paper three configurations of the gas inlet system are presented (**Figure 3**).

In the first configuration, the CO_2 flow is introduced from the top of the discharge zone through a gas shower **Figure 3(a)**). This configuration will be further referred to as "*direct flow configuration*". The temperature of the afterglow is monitored via a thermocouple installed downstream of the reactor.

In the second case, the gas flow direction is opposite: CO_2 is filling the vacuum chamber first and then entering the discharge tube from the bottom (**Figure 3(b)** "*reverse configuration*"). After passing the plasma zone, the hot gas is directed through a water-cooled gas shower at the top. The gas inlet device depicted in **Figure 1** and **Figure 3(b)** has an adjustable position, i.e. it can be fixed along the vertical axis. For the reverse configuration, the gas inlet device is placed in the proximity of the plasma zone to stabilize the discharge, but it is not connected to the gas feed.

In the third case (**Figure 3(c),**"*vortex configuration*"), CO_2 is supplied to the discharge zone through a tangential gas inlet at the bottom (also depicted in **Figure 1**). This stainless steel swirl gas inlet has four 3 mm holes in the tangential direction in order to create a vortex flow pattern. The processed gas is also directed through the water-cooled gas shower at the top. The afterglow temperature was measured with a thermocouple installed after the gas shower, similar to the case of the "reverse" set-up.

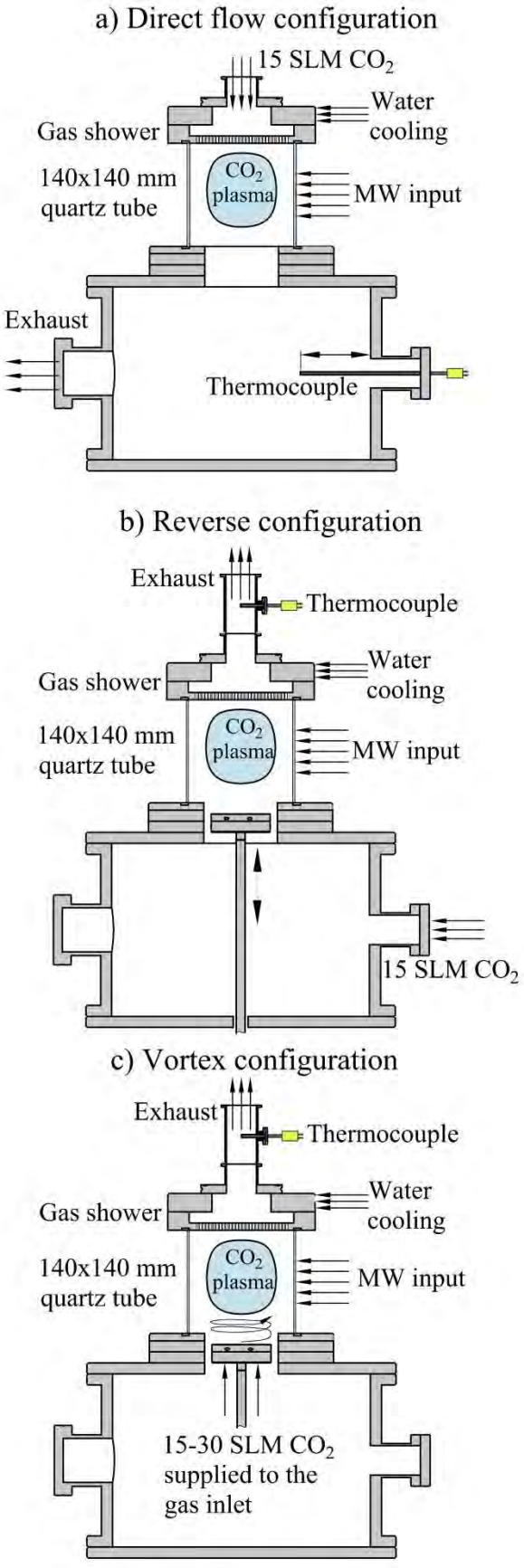

Figure 3.Various gas input configurations of the MW plasma reactor.

2.4 Computational fluid dynamics (CFD) simulations

CFD simulations of the gas flow dynamics are performed to analyse the vortex flow configuration, using the commercial software package COMSOL Multiphysics [40]. The study is carried out on this particular configuration to prove the formation of a vortex flow and to reveal the effect of turbulence.

The gas flow is computed using the k-ε Reynolds averaged Navier Stokes equations turbulence model [41]. This model is one of the most commonly used turbulence models that can compute flows for high degrees of turbulence. It is a two-equation model that solves the mass and momentum continuity partial differential equations:

$$\nabla.\left(\rho\overrightarrow{u_g}\right) = 0 \tag{5}$$

$$\rho\left(\overrightarrow{u_g}.\nabla\right)\overrightarrow{u_g} = \nabla.\left[-p\vec{I} + (\mu+\mu_T)\left(\nabla\overrightarrow{u_g} + \nabla\left(\overrightarrow{u_g}\right)^T\right) - \frac{2}{3}(\mu+\mu_T)\left(\nabla.\overrightarrow{u_g}\right)\vec{I} - \frac{2}{3}\rho k_T\vec{I}\right] + \vec{F} \tag{6}$$

where ρ stands for the gas density, $\overrightarrow{u_g}$ is the gas flow velocity vector, superscript T stands for transposition, p is the gas pressure, μ is the dynamic viscosity of the fluid, μ_T is the turbulent viscosity of the fluid, k_T is the turbulent kinetic energy, $\vec{I}$ is the unity tensor and $\vec{F}$ is the body force vector. Next to this, the model introduces two additional dependent variables, i.e., the turbulent kinetic energy, k, and the turbulent dissipation rate, ε, for which additional transport equations are solved. More details about these equations can be found in [41].

The k-ε model is coupled to a heat transfer model that solves the thermal balance equation:

$$\rho C_p\frac{\partial T_g}{\partial t} + \rho C_p\overrightarrow{u_g}\cdot\nabla T_g - \nabla\cdot\left(k_g\nabla T_g\right) = Q \tag{7}$$

where ρ is the gas density, C_p is the heat capacity of the gas, k_g is the thermal conductivity of the gas. T_g is the gas temperature and Q accounts for the gas heating.

In higher turbulent flows, turbulence results in a turbulent thermal conductivity, which together with the temperature dependent laminar thermal conductivity forms the effective thermal conductivity, and has an additional cooling effect on the gas. The effect of an increased heat flux due to turbulences in the system is accounted for by the Kays-Crawford model [42].

The vortex gas flow is simulated only in the microwave discharge tube to limit the calculation time, and because this is the domain of interest, and the rest of the geometry will not affect the flow in that region. It is important to mention that significant computational time and resources are needed to accurately describe the flow by means of eddy viscosity, because of the required very fine grid of the geometry meshing. This was outside the scope of this paper, as the simulations are meant to support and explain the experimental data. Therefore, we used a more approximate k-ε model. Although the exact values of velocity and turbulent heat conductively might not be very accurate, we believe that the flow pattern and the turbulent heat viscosity estimations based on this model are sufficient for the verification of the vortex regime formation. Indeed, it was stated in the of Gronald *et al.* [43] that unsteady Reynolds averaged Navier Stokes (RANS)-based simulations on a relatively coarse grid can provide reasonable and industrially relevant results with limited computational effort.

3 Results and discussion

3.1 Effect of the pressure

The CO_2 conversion and energy efficiency of the process are plotted as a function of gas pressure in **Figure 4**, for the three different gas inlet configurations of the MW plasma reactor**.** Both the MW power (4.75 kW) and gas flow rate (15 SLM CO_2) are kept constant,

and thus the energy input, SEI, was also fixed (i.e., 4.8 eV/molec). Note that the energy efficiencies plotted here are all determined with the input power, as mentioned above. If they would be calculated with the plasma power, as often done in the literature, they would all be 5-10% higher, as the plasma power is typically 5-10% lower than the input power. All these configurations exhibit a drop of the conversion and energy efficiency upon increasing pressure, consistent with model calculations [19]. However, remarkable differences in maximum conversion for the various gas inlet regimes are observed. Indeed, the direct configuration yields a conversion of 3.5% at 200 mbar, while values of 38.2% and 23.8% are measured for the reverse and vortex systems at the given conditions, respectively. The energy efficiency exactly follows the trend of the conversion, because the SEI is kept constant.

Furthermore, as the drop in conversion and energy efficiency is more pronounced for the reverse configuration than for the vortex setup, it is interesting to note that the reverse configuration is more efficient at 200 mbar (with conversion of 38.2% and energy efficiency of 23.1%, vs 23.8% and 14.2% for the vortex regime), while the vortex regime exhibits a higher conversion and energy efficiency at 1 bar (i.e., conversion of 11.3% and energy efficiency of 6.9%, vs 6.2% and 3.7% for the reverse configuration).

The drop in conversion and energy efficiency upon increasing pressure in the MW discharge is somewhat expected. First of all, it is known that at atmospheric pressure the rotational and vibrational temperatures of the MW plasma are in thermal equilibrium [44]. This leads to a high gas temperature. At the same time, the most efficient mechanism of CO_2 decomposition, i.e., through vibrational excitation of the asymmetric mode of CO_2 [20], becomes less dominant with higher temperature and pressure [19]. This effect is explained by the depletion of the high vibrationally-excited CO_2 molecules through vibrational-translational relaxation, stimulated by both pressure and temperature. In addition, the drop in

conversion and energy efficiency in a MW plasma reactor at higher pressure can also be attributed to the CO recombination reactions 8 and 9:

$$CO+O+M \rightarrow CO_2+M \quad (8)$$

$$CO+O_2 \rightarrow CO_2+O \quad (9)$$

It was demonstrated by Berthelot *et al.* that the rates of reaction 8 and 9 increase with temperature and pressure, thus indeed limiting the CO_2 conversion [19].

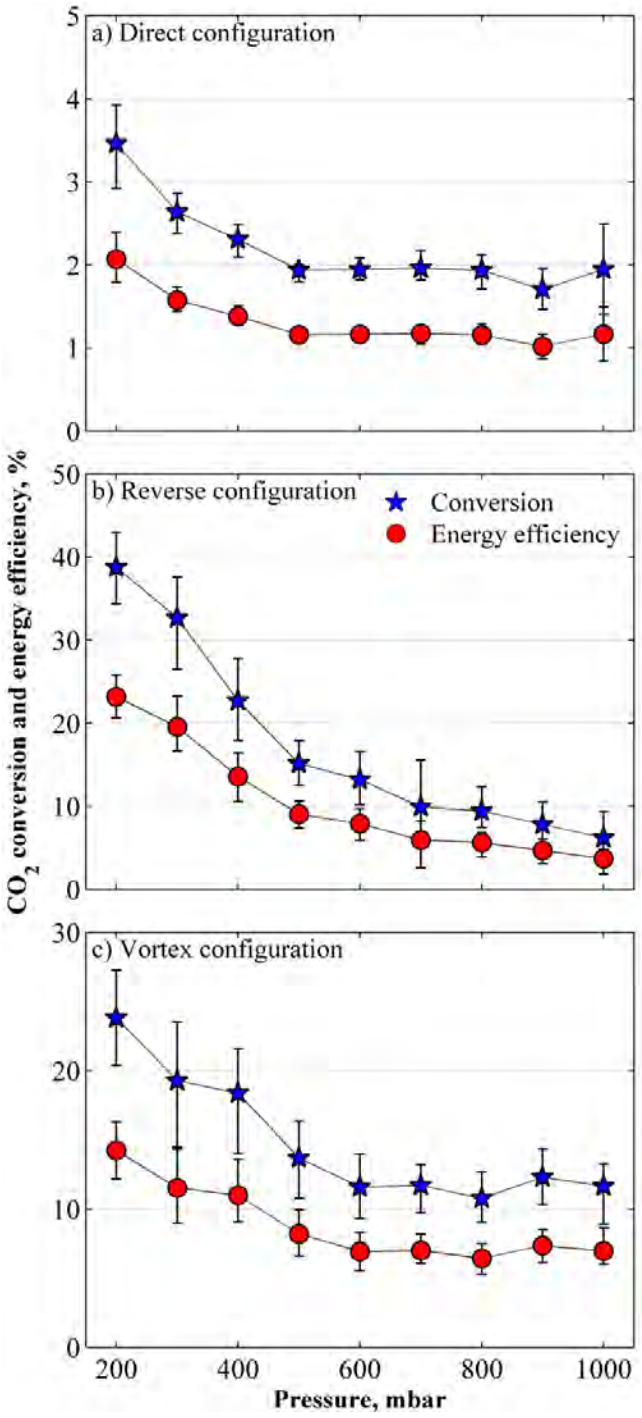

Figure 4. CO_2 conversion and energy efficiency obtained in the MW plasma at 4.75 kW input power and 15 SLM CO_2 gas flow rate (corresponding to an SEI of 4.8 eV/molec), for the three different gas inlet configurations, upon increasing the pressure.

3.2 CO_2 conversion in the MW discharge at 200 mbar

It is interesting to note that the largest difference in CO_2 conversion and energy efficiency for the various gas inlet configurations of the MW discharge was observed at 200 mbar (cf. **Figure 4**). To further investigate this effect, the reverse and vortex configurations are compared, while varying the flow rate and power input (**Figure 5**). We perform this comparison at 200 mbar, where a stable discharge could be sustained in a wide range of process parameters for both gas inlet regimes. For the reverse configuration, a higher power or a lower flow rate result in a proportional rise of the conversion, which is like expected. The effect is opposite for the energy efficiency, which is also like expected, based on equations (3-4), although the flow rate of 15 SLM still gives a slightly higher energy efficiency than the flow rate of 20 SLM. Thus, a flow rate of 15 SLM CO_2 and 3.75kW input power yields the highest energy efficiency of around 25%. On the other hand, in the vortex configuration, the flow rates of 15 and 20 SLM CO_2 yield rather similar conversion. As a result, the regime with 20 SLM is more efficient than 15 SLM, with the highest energy efficiency of 26% at 2.75 kW MW power input. This behavior is consistent to our observation of the vortex configuration in the 200-1000 mbar pressure range presented further (cf. **Figure 6**). The conversion at 20 SLM is quite similar in both the vortex and reverse configuration, but the latter configuration yields a much higher conversion at 15 SLM, as was also obvious from **Figure 4** above.

Remarkably, when a CO_2 flow rate of 5 SLM is applied at high power (>3.75 kW), the conversion appears to be much higher in the vortex gas inlet configuration. At 4.75 and 5.75 kW power input, conversions of 69% and 75% (with energy efficiencies of 14% and 12%, respectively) were measured for the vortex configuration, vs. 50% and 53% (corresponding to energy efficiencies of 9.8% and 8.7%) for the reverse configuration, respectively. Moreover, the 5 SLM vortex flow regime is more efficient than the reverse flow regime for the entire

power input range, with maximum energy efficiency of 14% at 2.75 kW MW power, corresponding to 41% conversion, while the reverse configuration yields 12% energy efficiency with a conversion of 34% for the 5 SLM – 2,75 kW discharge.

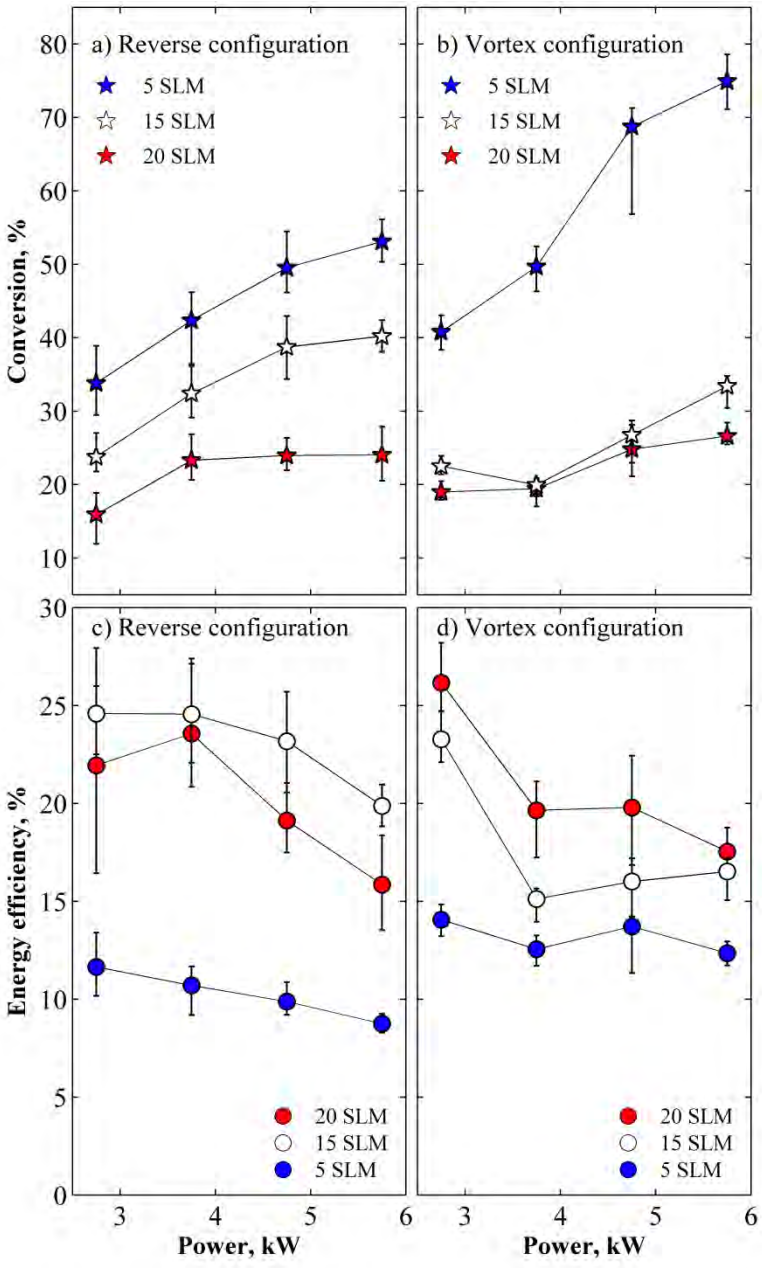

Figure 5. CO_2 conversion and energy efficiency in the MW plasma in reverse (a,c) and vortex configurations (b,d), as a function of input power, at 200 mbar and three different gas flow rates.

3.3 Effect of the flow rate in the vortex configuration

The aim of this work is to target the operation of a stable MW discharge in a wide (200-1000 mbar) pressure range and a wide range of gas flow rates. For the direct and reverse configuration, however, a stable discharge in this entire pressure range can only be achieved in a narrow window of process parameters (15 SLM CO_2 – 4.75 kW). For instance, it is not possible to sustain a reliable discharge at pressures above 500 mbar when applying a CO_2 flow rate higher than 15 SLM in the direct and reverse configuration. In contrast, the vortex gas inlet regime allowed various flow rates (between 15 and 30 SLM CO_2) to be tested (cf. **Figure 6**). A vortex gas flow regime is utilized before in MW plasma systems to avoid overheating of the reactor walls [21, 23] and allows to operate the MW plasma in a wider regime of conditions. Interestingly, it can be deduced from **Figure 6** that the MW plasma in vortex configuration yields a very similar conversion in the entire range of gas flow rate investigated, i.e., from 15 SLM to 30 SLM. This is quite remarkable, because a drop in conversion upon increasing flow rate is usually observed at constant power in most plasma experiments [5, 7, 13, 15], although the non-linear influence of flow rate on the CO_2 conversion was also reported for MW plasmas in CO_2+H_2 gas mixtures [32], a CO_2 RF discharge [45] and gliding arc plasmatron reactors [8, 9]. This effect might be attributed to the complex interplay between the vortex gas pattern, the non-uniform absorption of MW power and the chemistry of CO_2 decomposition.

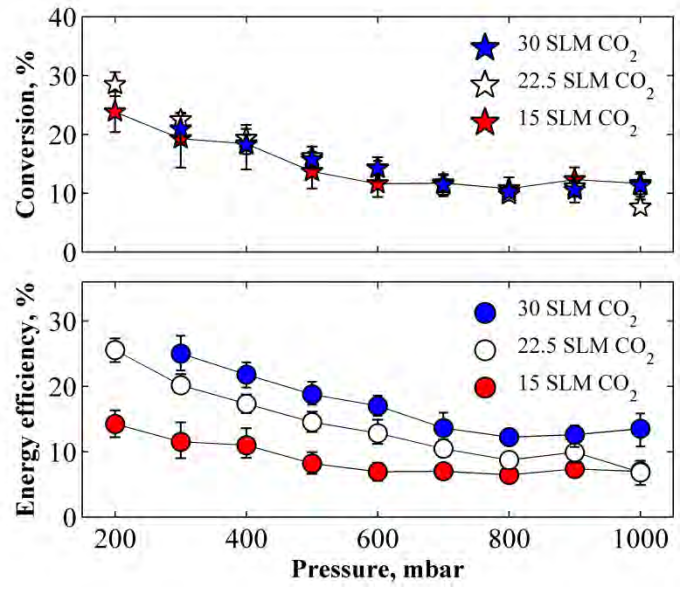

Figure 6. CO_2 conversion and energy efficiency in the MW plasma in the vortex configuration as a function of pressure, at a MW power of 4.75 kW and three different flow rates (15, 22.5 and 30 SLM).

As the conversion appears to be independent of the gas flow rate, the energy efficiency obviously rises substantially upon higher flow rates, as can be explained from equations (3-4) above, reaching values of 11.5%, 20.1% and 25%, for 15, 22.5 and 30 SLM CO_2, respectively, at 300 mbar. A further increase of the flow rate is not feasible due to pumping limitations. For the same reason, the lowest pressure feasible at 30 SLM CO_2 flow rate is only 300 mbar.

CFD calculations are used to verify the formation of the vortex gas pattern in this configuration of the MW discharge system and also to analyse the effect of rising gas flow. In **Figure 7**, the gas velocity streamlines are plotted for a flow case with 600 mbar pressure at 30 SLM inlet flow rate. It can be observed that multiple vortices form in the discharge tube. **Figure 8** shows that these vortices are organized in three distinct regions. An outer vortex moves upwards at a high velocity, after which a part of the flow recirculates back downwards. In the center of the tube, the flow moves back upwards at a low axial velocity

magnitude. This axial flow pattern remains the same, regardless of the applied pressure or flow rate in the system, as is shown in **Figure 9**.

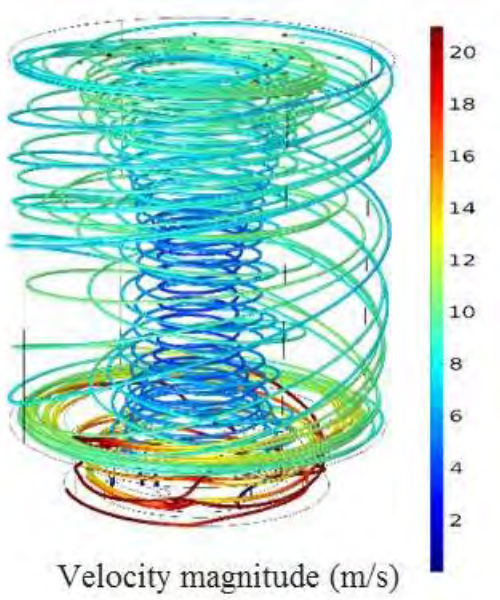

Figure 7. Gas velocity streamlines, for a flow rate of 30 SLM at a pressure of 200 mbar.

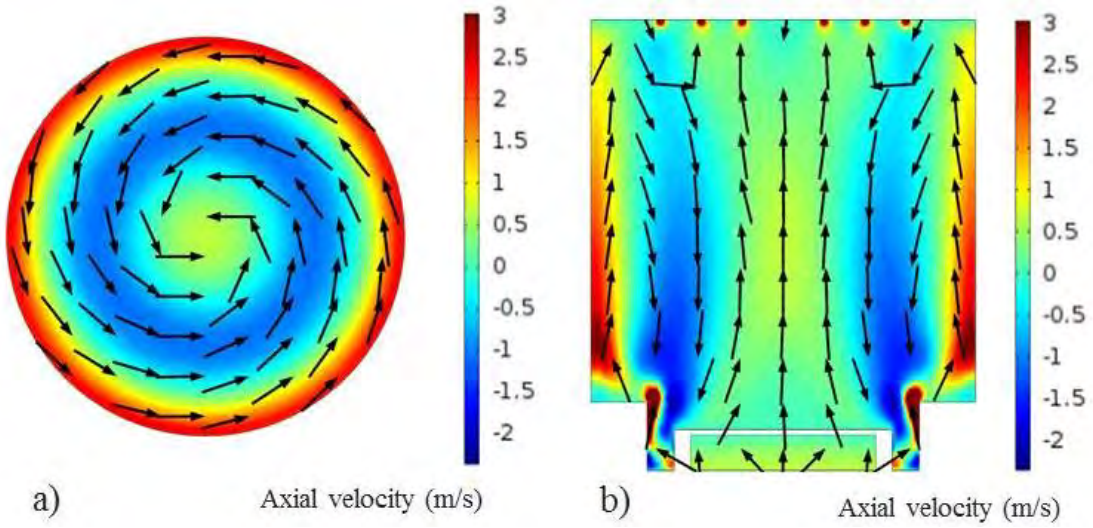

Figure 8. Axial velocity (m/s) and normalized flow directions (black arrows) for 200 mbar pressure at 30 SLM for (a) a horizontal cut through the reactor and (b) a vertical cut through the reactor.

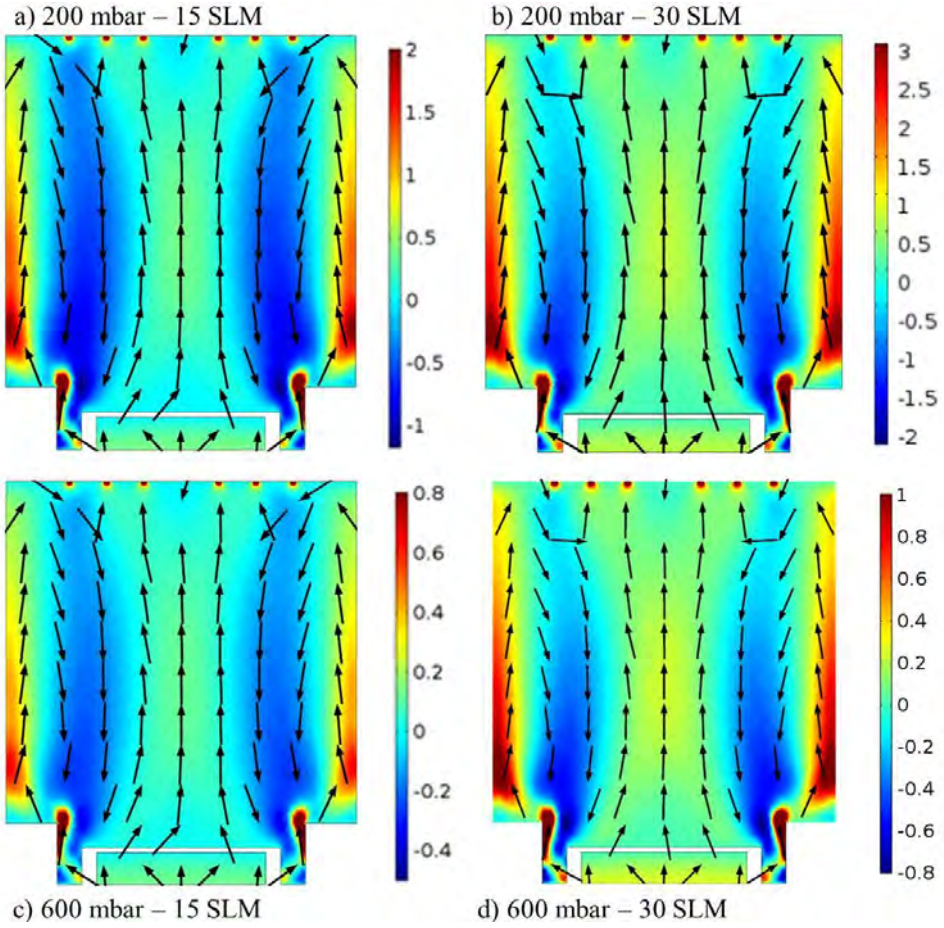

Figure 9. Axial velocity (m/s) and normalized flow directions (black arrows) for 200 mbar pressure at (a) 15 SLM and (b) 30 SLM and for 600 mbar pressure at (c) 15 SLM and (d) 30 SLM.

Figure 10 shows the turbulent thermal conductivity for different pressures and flow rates in the reactor. The value for the turbulent thermal conductivity is significantly higher than the laminar value (i.e., 0.0166 $\frac{W}{m\,K}$), which means that the higher degree of turbulence that manifests itself in this configuration will have an important cooling effect on the plasma. Comparing **Figure 10** (**a)** and **(b)** (or **Figure 10 (c)** and **(d)**), it can be observed that an increase in flow rate results in an increased effective thermal conductivity, while comparison between **Figure 10 (a)** and **(c)** (or **Figure 10 (b)** and **(d)**) indicates that a pressure difference does not affect the effective thermal conductivity significantly. The

higher turbulence, due to a higher flow rate, will result in higher turbulent cooling of the gas, and thus of the plasma. This additional cooling effect has also been shown to play a determining role in a reverse vortex flow gliding arc plasmatron [46]. The resulting decrease in temperature of the plasma lowers the rates of vibrational-translational relaxation, which is an effective energy loss mechanism for the higher vibrational levels of CO_2 and thus a limiting process for energy efficient CO_2 conversion in microwave plasmas [19]. Hence, the cooling due to the higher turbulence (at higher gas flow) might explain the higher CO_2 conversion and energy efficiency, as illustrated in **Figure 6**. In addition to that, the post-discharge temperature measurements presented in the next section (and especially in **Figure 13**) can be associated with the concept that the enhanced turbulence cooling can lower the gas temperature of a high pressure MW plasma.

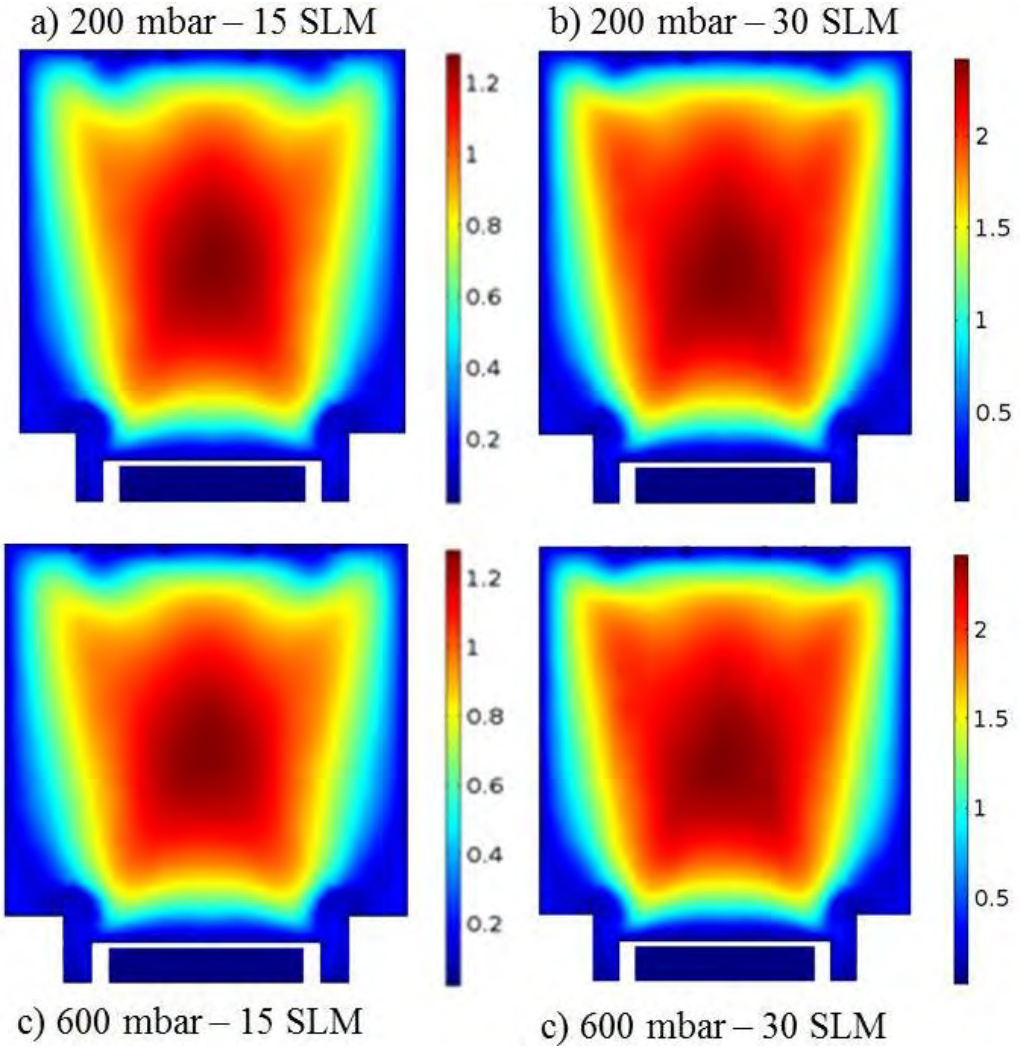

Figure 10. Effective thermal conductivity (W/(m*K)) for 200 mbar pressure at (a) 15 SLM and (b) 30 SLM and for 600 mbar pressure at (c) 15 SLM and (d) 30 SLM.

3.4 Post-discharge temperature measurement

It is known that the downstream processes significantly influence the overall efficiency of the CO_2 conversion process and that they are governed by the pressure and temperature dependent CO recombination reactions 8 and 9 [19]. Hence, a pressure increase and a post-discharge cooling will have a prominent influence on the MW discharge reactor exhaust properties and thus on the efficiency of CO_2 conversion. To investigate these effects, we measure the temperature downstream of the MW discharge reactor in all three gas flow

configurations (cf. **Figure 3**) upon increasing the pressure. For the direct gas inlet configuration, the thermocouple is placed at different radial positions inside the vacuum chamber and 20 cm below the MW plasma reactor itself (cf. **Figure 3**), and the data obtained (**Figure 11)** illustrate that the exhaust temperature decreases when moving away from the chamber axis and when the pressure increases. Although the temperature is measured 20 cm below the MW plasma reactor, still values as high as 1000 K are obtained at 200 mbar, at 4 cm from the axis. The indication "discharge zone" in **Figure 11** represents the area close to the reactor axis (~3 cm) where the thermocouple induces an additional discharge. Therefore, the temperature cannot be measured in this area. It is important to realize that, because the thermocouple is positioned 20 cm below the MW plasma reactor itself, the values presented in **Figure 11** will be affected by the heat exchange processes in this area. Inside the plasma reactor (and also directly in the afterglow), the gas temperature will even be much higher, certainly at higher pressure, as revealed among others by computer modeling [19]. The influence of the heat exchange processes on the exhaust temperature of the direct configuration will be discussed below.

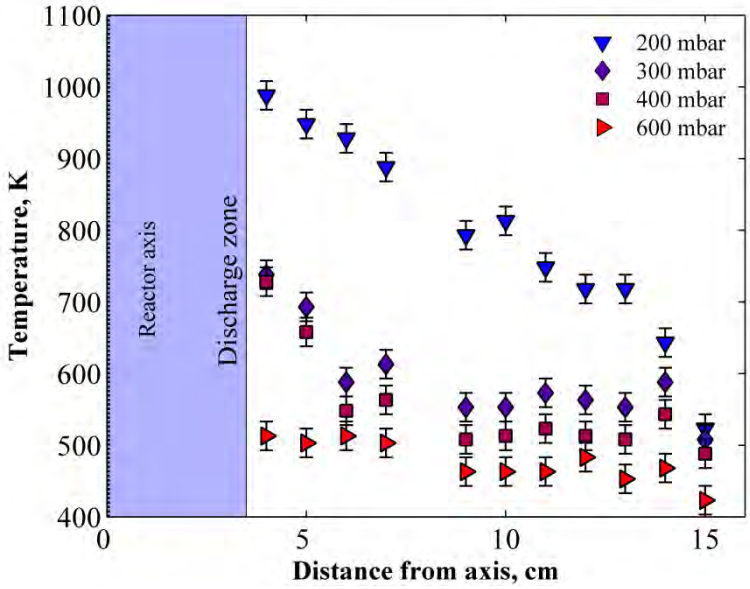

Figure 11. Temperature distribution as a function of distance from the central axis, measured in the vacuum chamber, at a position 20 cm downstream of the MW discharge reactor (see **Figure 3 (a)**), for the direct gas inlet configuration, at a power of 4.75 kW and a flow rate of 15 SLM.

The pressure dependence of the exhaust temperature for the direct, reverse and vortex configurations is presented in **Figure 12**. For the reverse and vortex configuration the temperature is probed ~5 cm after the cooling stage (cf. **Figure 10**). The exhaust is substantially cooler in these cases at lower pressures, compared to the direct flow configuration that is operating without any quenching. At 200 mbar, values almost twice as high are achieved for the direct configuration compared to the reverse and vortex regimes (988 K vs 563 and 535 K, respectively). However, the temperature downstream of the reverse and vortex set-up increases with pressure. At 1 bar, temperatures of 788 K, 673 K and 473 K are measured for the vortex, reverse and direct configurations, respectively.

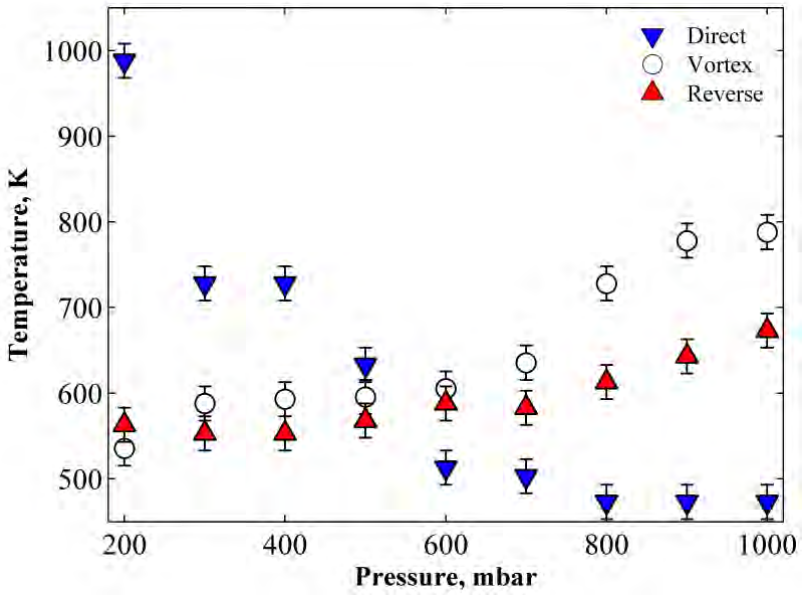

Figure 12. Exhaust temperature measurements for the direct, reverse and vortex gas inlet configurations of the MW plasma reactor, as a function of pressure, at a MW power of 4.75 kW and gas flow of 15 SLM CO_2.

In case of the vortex configuration, we also investigated the effect of the flow rate (**Figure 13**). This is not possible in case of the direct and reverse configurations, where a stable plasma is only reached in a limited range of conditions, as mentioned above. Interestingly, increasing the flow rate has limited influence on the exhaust temperature of the vortex regime at lower pressures (up to 700 mbar), while the difference becomes more prominent closer to atmospheric conditions. The exhaust temperature of the MW discharge with 15, 22.5 and 30 SLM CO_2 supplied to the MW plasma reactor through the vortex gas inlet at 1 bar equals 788 K, 743 K and 683 K, respectively. The reason for this behavior might be attributed to the fact that the specific power input is decreasing with rising gas flow rate and to the enhanced turbulence cooling at higher vortex gas flow rate, demonstrated by CFD simulation in the previous section.

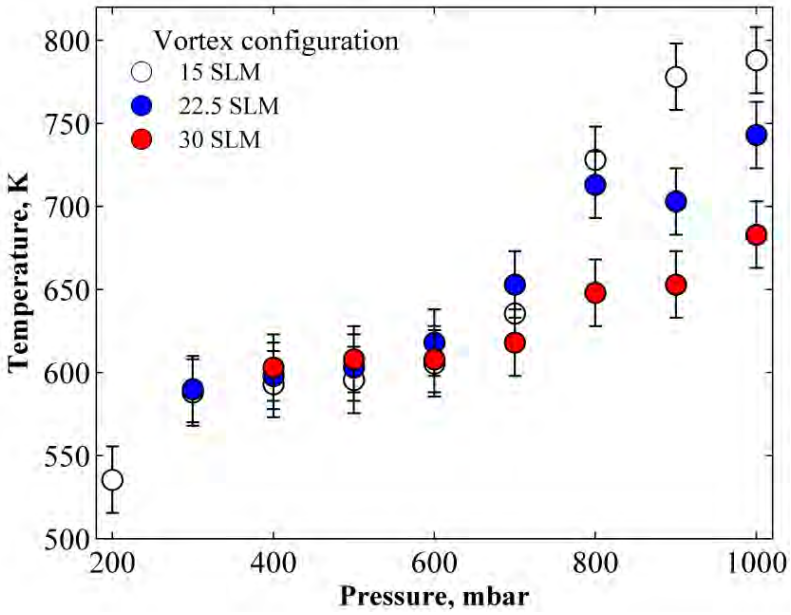

Figure 13. Post-discharge temperature measurements for the vortex gas inlet configurations of the MW plasma reactor, as a function of pressure and gas flow, at a MW power of 4.75 kW.

The afterglow temperature measurements allow us to obtain a better understanding of the poor performance of the MW discharge operating in the direct gas flow configuration, even at low pressure (cf. **Figure 4**). Indeed, in this case, temperatures up to 1000 K are measured downstream of the reactor. In reality, the values in the discharge afterglow will be even higher, because the thermocouple could only be placed at a certain distance from the reactor axis (i.e., above 4 cm) and quite far away from the plasma reactor (i.e., 20 cm) (cf. **Figure 3** and **Figure 12**). It is thus clear that inside the plasma reactor, the temperatures will be much higher, as also revealed from model calculations [19].

In case of the reverse and vortex flow configurations, the temperature inside the plasma will also be high, but the cooling step installed downstream the reactor in these two configurations allows a decrease of the exhaust temperatures down to ~550 K at 200 mbar. The higher conversion achieved in these regimes compared to the direct configuration (cf. **Figure 4**) might thus be attributed to the lower temperature in the afterglow. It was

demonstrated by Berthelot *et al.* that even at 200 mbar the reaction rate of CO recombination (Reaction 8) increases when the temperature rises from 300 K to 1000 K [19]. In this way, we can argue that the excessive exhaust temperatures of the direct configuration of the MW discharge reactor highly limit the performance of this system for CO_2 conversion, while the introduction of a quenching step downstream in case of the vortex and reverse gas flow inlet configurations allows to obtain substantially higher conversions and energy efficiencies. However, in **Figure 12** it can be noted that rather high temperatures (up to 700-800 K) are still achieved downstream the reverse and vortex configurations at higher pressures. This may indicate that the cooling rate is not sufficient in these cases and thus that the CO_2 conversion and energy efficiency in these systems can be further enhanced by improving the exhaust cooling system. Some possibilities to achieve this would be the introduction of another cooling stage or increasing the contact time of the exhaust gas in the quenching step. Besides that, to have a better understanding of the MW discharge thermalisation with rising pressure, it would be useful to apply optical emission spectroscopy (OES) inside the plasma reactor. By means of OES it is possible to estimate the vibrational and rotational temperatures of the plasma and thus to analyze how close they are to thermal equilibrium [44].

It is also interesting to observe the influence of rising pressure on the exhaust temperature of the MW discharge in the direct flow configuration. In general, the gas temperature of a MW plasma is expected to increase upon increasing pressure [19, 44]. This is indeed observed when studying the exhaust temperature of the MW discharge in the reverse and vortex gas flow configurations (cf. **Figure 12**). At first glance it may seem that the opposite is the case for the direct gas inlet configuration. However, we need to keep in mind that the values presented in **Figure 11** and **Figure 12**.for the direct flow set-up are measured only at a distance of 20 cm from the MW plasma and at least 4 cm from the central axis. Hence, this is quite far in the afterglow, or even beyond the afterglow of the plasma. It should

be noted that these values are highly affected by heat exchange processes occurring in the chamber downstream of the reactor. Indeed, we might expect that the flow expansion in the vacuum chamber will induce convective heat transfer, thus decreasing the exhaust temperature at that point. This process will be highly dependent on the chamber pressure and turbulence formed after the gas expansion. This can probably explain the downward trend of the post-discharge temperature upon increasing pressure, observed in **Figure 11** and **Figure 12**.

4 Analysis and comparison with literature results

A summary of our CO_2 conversion experiments for the various conditions investigated in the three different configurations of the MW discharge reactor is presented in **Figure 14** and in **Table 1**. As stated before, the conversion and energy efficiency almost linearly drop upon increasing the pressure, regardless of the gas inlet configuration, although the drop is more pronounced for the reverse configuration. At an SEI of 4.8 eV/molec, which is realized at a MW power of 4.75 kW and a flow rate of 15 SLM, the direct configuration yields the lowest conversion and energy efficiency in the whole pressure range studied. This can be explained by the lack of downstream cooling. Indeed, as we can see in **Figure 3(a)**, the heated exhaust mixture of the CO_2 discharge products expands into the vacuum chamber after passing through the discharge zone. In contrast to that, the reverse and vortex gas inlet configurations (**Figure 3(b)** and **(c))** have a quenching stage downstream of the plasma zone. The importance of post-discharge quenching was underlined in a number of papers [20, 23] and it was already stated, based on model predictions, that the CO recombination reactions 8 and 9 are more prominent at higher temperature [19].

In our study a conversion of 39% with a corresponding energy efficiency of 23% is achieved in the reverse flow configuration at 200 mbar and a CO_2 flow rate of 15 SLM. A somewhat higher energy efficiency, i.e., 25%, is obtained in the vortex flow configuration when 30 SLM CO_2 was supplied at 300 mbar, corresponding to a conversion of 20%. Interestingly, the same flow configuration also demonstrates the best performance at atmospheric pressure: energy efficiencies of 14% and 12% are achieved, with a corresponding conversion of about 12%, at 30 and 15 SLM CO_2 flow rate in the vortex configuration at 1 bar, while an energy efficiency of only 3.7%, with a conversion of 6.2%, is obtained in the reverse configuration. Besides that, the 5 SLM CO_2 vortex regime at 200 mbar and MW

power of 5.75 kW demonstrates the opportunity to obtain a very high conversion of up to 75% with an energy efficiency of 12.3%. To benchmark our results, we compare them with the data reported in literature for the CO_2 decomposition in MW discharges at various conditions; see **Table 1**.

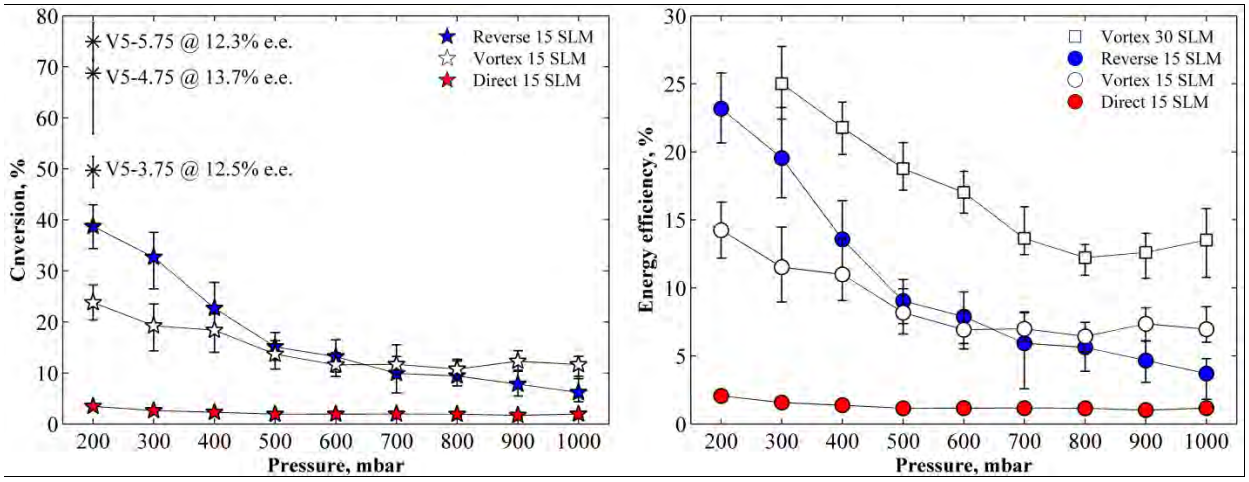

Figure 14. CO_2 conversion and energy efficiency in the MW plasma at 4.75 kW – 15 SLM (4.8 eV/molec) for the three different gas inlet configurations, upon increasing pressure. For the vortex configuration, the energy efficiency is also plotted at 30 SLM, while the values for the conversion as the same as at 15 SLM. Besides that, the conversion is presented for 5 SLM vortex gas flow at 200 mbar upon increasing power. In this case the regime is designated as "V5-**X**@ **Y**% e.e.." where **X** is power in kW and **Y** is the corresponding energy efficiency. For the other configurations, no results are presented at other flow rates, because no stable plasma could be sustained in this wide pressure range.

Operation at lower pressures makes it possible to fully exploit the non-equilibrium character of the MW plasma, with the potential to reach higher conversion and energy efficiencies [20]. It was demonstrated in our work, but also by modeling [19] and in a number of experiments from literature [23, 35] that the pressure range between 150 and 300 mbar yields the higher conversion and energy efficiency, as it allows to utilize the most favorable CO_2 dissociation kinetics through the CO_2 vibrational levels [19]. Indeed, the highest energy efficiencies ever reported (~90%) for CO_2 MW plasma systems were obtained at these conditions, although this was also in combination with supersonic gas flow [22]. An advantage of operation at these moderate pressures is that only relatively cheap fore-vacuum

pumps (cf. for instance the vacuum scheme in **Figure 2**) are required. However, the operational cost of such technology is still high, mostly due to the vacuum system energy consumption, and it may hinder the scale-up of the process.

Therefore, in a number of papers, operation at atmospheric pressure is targeted [27, 28, 44, 47]. Although it is known that the MW plasma is (nearly) in thermal equilibrium in this case, the atmospheric pressure systems have the undeniable advantage of vacuum-free operation. The data reported in literature for CO_2 conversion in MW plasmas at atmospheric pressure appear to be quite promising, with rather high energy efficiencies or conversions (although the combination of both is still limited). An interesting idea was elaborated in a series of articles by Hong *et al.* [27, 47], where the CO_2 activated in a MW plasma was utilized as an oxidant for Zn or coal powders that were introduced downstream of the MW plasma, and reacted as "M" in reaction 10:

$$CO_2^* + M \rightarrow CO + MO_x \quad (10)$$

It is worth noticing that this process is not catalytic, as the interaction with material consumes oxygen and thus changes the stoichiometry of the reactants. As presented in **Table 1**, this approach allows to achieve a conversion of 30-45%, with a corresponding energy efficiency of 14-8%, depending on the conditions.

Remarkably, Mitsingas *et al.* reached an energy efficiency of 50-80% in an atmospheric pressure MW plasma reactor, but the conversion was only around 9-3% [28]. The high energy efficiency obtained in the compact discharge formed between an 8 mm inner diameter nozzle and a 2.4 mm tungsten electrode can be attributed to the high plasma density, which is known to be beneficial for the CO_2 conversion, due to efficient population of the CO_2 vibrational levels [19].

An important remark regarding MW reactors operating at atmospheric pressure is that the ignition of the MW discharge at these conditions requires the implementation of electric field concentrators [28] or large argon admixtures [44]. In our case the discharge is ignited at lower pressure (~100 mbar) without such ignition assistants also due to the rather high MW power input applied in this study. Besides that, the data in literature, as well as presented in our work, indicate that there is a trade-off between the energy efficiency and conversion. Hence, at rather low conversion, the cost of product purification and separation would be a big issue for process up-scaling, even if the energy efficiency of the plasma process itself is rather high. Novel ways to improve the overall efficiency of the technology should be considered.

The introduction of a catalytic step might be interesting, to utilize the relatively hot exhaust mixture that was previously activated in the MW plasma (cf. **Figure 7 and 8** above). Post-discharge treatment of the CO_2 MW plasma reactor exhaust via a catalytic step was demonstrated by Chen *at al.* [24-26] and allowed a twofold increase of the conversion and energy efficiency (i.e., from 20% to 42% conversion and energy efficiency). Remarkably, the catalyst was pre-treated via a MW argon plasma in the same vacuum chamber prior to the CO_2 decomposition reaction. Interestingly, Spencer *et al.,* also implemented a catalyst downstream of an atmospheric pressure MW reactor, but this resulted in a drop of the conversion and energy efficiency [44]. This underlines that also unwanted reverse reactions can be catalyzed in the post-discharge step of MW plasma systems.

The introduction of hydrogen-containing admixtures, like H_2 [32, 33] or H_2O [25, 26], affects the plasma parameters, such as gas and electron temperature, and it allows the generation of syngas as a product. The advantage of this approach is that water is easily available, while H_2 can be generated via another technology that consumes renewable electrical energy, i.e., electrolysis. Another suitable hydrogen-source gas could be CH_4, thus

allowing the use of biogas as feed gas, but the number of papers on the combined CO_2/CH_4 conversion in a MW plasma is very limited [5].

The results in the literature are somewhat better than the ones presented here. First, we repeat here that the energy efficiencies reported in this work are obtained based on the input power input, and when we would calculate them from the plasma power, as often done in literature, they would be ca. 5-10% higher. Furthermore, the somewhat lower performance in our setup can also be attributed to the fact that a MW plasma reactor should be designed for utilization at a certain pressure and gas flow regime. In our study, the aim is not to obtain the highest possible conversion and energy efficiency, but to target a stable discharge operation in a wide pressure range and with several gas inlet configurations, to obtain more insight in the underlying mechanisms in this wider range of operating conditions, and this is realized by means of the rather large volume MW plasma system. However, it is known that high-density plasmas (and thus low-dimensional devices) are beneficial for CO_2 conversion [19]. Nevertheless, such systems would not allow the versatility of our reactor. For instance, puncturing of the quartz tube is often observed in a MW discharge operating at high power per unit wall area without vortex flow gas feed [21]. In this way, it would not be possible to test the direct and reverse flow regimes that are demonstrated in our study in the whole pressure range of 200 mbar - 1 bar. Therefore, the operational regime (low or atmospheric pressure) and gas flow configuration (forward or vortex flow) should be chosen during the design stage in order to assemble an efficient system. This is, however, not the primary aim of the current paper.

It is important to notice that the measurements of the CO_2 conversion in our case (and in most of the presented literature) have an *ex-situ* character, i.e. the gas is sampled at the reactor exhaust. It is demonstrated above that downstream processes are crucial for the process efficiency, as the CO recombination reactions can dominate in the hot afterglow of

the CO_2 MW plasma. Therefore, *in-situ* diagnostics [29, 35] are required to better understand and control the operation of the discharge systems. Besides that, efforts to decrease the gas temperatures and thus the recombination reaction rates, while increasing the power density of the plasma, should have a positive impact on the energy efficiency of the process [48]. In practice, this can be realized by discharge pulsing [49], *in-situ* extraction of oxygen [50, 51] and decreasing the reactor dimensions [28], although the latter will not be beneficial in terms of throughput or upscaling.

Table 1. Summary of CO_2 conversion performance in different MW plasma reactors and for various discharge configurations and conditions

Pressure, mbar	Conversion %	Energy efficiency %	SEI, eV/molec.	Specifications	Reference
200	74.9	12.3	17.5	V5-5.75[1]	This work
200	38.7	23.1	4.8	R15-4.75[2]	This work
300	20.9	25	2.4	V30-4.75[3]	This work
1000	11.6	13.5	2.4	V30-4.75[3]	This work
90	20	35	1.9	Forward flow	[29]
20	65	8	22.9	Pure CO_2, forward flow	[32]
20	~85	6	5.8	H_2/CO_2=3, forward flow	[32]
40	20	20	2.9	Only MW	[26]
40	42	42	2.9	MW+catalyst	[26]
200	~10	~90	0.3	Supersonic flow	[20]
127	~ 15	~ 50	~ 1	Vortex flow	[35]
212	~ 8	~ 40	~ 0.5	Vortex flow	[35]
200	83	24	10.3	Supersonic flow	[23]
200	47	35	3.9	Vortex flow	[23]
200	11	51	0.6	Vortex flow	[23]
1000	9	50	0.5	2 mm nozzle	[28]
1000	3	82	0.1	2 mm nozzle	[28]
1000	~45	~ 8	4.5	MW+ Coal oxidation	[27]
1000	~32	~14	4	MW+ Coal oxidation	[27]
1000	10	20	1.4	CO_2 + Ar	[44]

[1]- Vortex configuration with supplied 5 SLM CO_2 flow rate and 5.75kW power input

[2]- Reverse configuration with supplied 15 SLM CO_2 flow rate and 4.75kW power input

[3]- Vortex configuration with supplied 30 SLM CO_2 feed flow and 4.75kW power input

5 Conclusion

The CO_2 conversion is studied in a MW discharge reactor in a wide pressure range (200 - 1000 mbar), exploring three different gas flow configurations, i.e., direct, reverse and vortex flow regimes. In the direct gas flow configuration, the exhaust of the plasma reactor expands into the vacuum chamber without additional cooling. Afterglow temperatures up to 1000 K are measured at quite some distance from the outlet, so the exhaust temperature is probably still higher, and this can explain the very low conversion and energy efficiency (~3.5% and 2% at 200 mbar, and even lower values at higher pressures) that are obtained, due to the lack of quenching of the exhaust, allowing the backward reaction (i.e., recombination of CO into CO_2) to occur at rather high rates. In the reverse flow configuration, the exhaust passes through a cooling stage during which quenching can occur. This regime results in the highest conversion (~38% at 200 mbar) obtained in this study (with a corresponding energy efficiency of ~23%), but the values drop significantly upon rising pressure. Finally, a vortex flow configuration is applied, which utilizes the same cooling and quenching approach as the reverse flow configuration, but in addition also a swirl flow pattern. The formation of the vortex in this case is verified by CFD simulations, which also demonstrate the effect of the enhanced turbulence cooling at higher gas flow rates. This configuration allows to operate the MW plasma in a wider range of conditions (flow rate and power) in the entire pressure range. Therefore, the highest energy efficiencies (~25% at 300 mbar and ~13% at 1 bar, for a corresponding conversion of 21% and 12%) are achieved in this regime. An almost linear drop of the conversion and energy efficiency is observed upon increasing pressure for all gas flow configurations, although it is somewhat less pronounced for the vortex flow configuration. This drop can be attributed to thermalisation of the plasma at increasing pressure, leading in turn to (i) less efficient CO_2 dissociation by the vibrational kinetics (due to more prominent relaxation

of the vibrational levels), and (ii) fast recombination of CO into CO_2. Analysis of the exhaust temperature reveals that the post-discharge cooling is crucial for the system performance in terms of conversion and energy efficiency, and should be further optimized. MW plasma systems operating at atmospheric pressure are probably the most interesting to be scaled-up, in spite of their lower conversion and energy efficiency, due to the vacuum-free operation conditions. From another point of view, the vortex configuration is the most promising, as it allows operation in a wider range of process parameters (flow, pressure, specific power input), and gives the best results at atmospheric pressure, which is most interesting for real applications. To further increase the conversion and energy efficiency of such systems, post-discharge treatment via catalytic or oxidative reactions can be implemented downstream, as demonstrated already in literature.

6 Acknowledgments

The research leading to these results has received funding from the European Union Seventh Framework Programme (FP7-PEOPLE-2013-ITN) under Grant Agreement № 606889 (RAPID - Reactive Atmospheric Plasma processIng – eDucation network).

7 References

[1] G. Centi and S. Perathoner, Opportunities and prospects in the chemical recycling of carbon dioxide to fuels, Catalysis Today 148 (2009) 191-205.

[2] J. Ren, F.F. Li, J. Lau, L. Gonzaílez-Urbina, and S. Licht, One-Pot Synthesis of Carbon Nanofibers from CO_2, Nano Letters 15 (2015) 6142-6148.

[3] A. Goede and R. van de Sanden, CO_2-Neutral Fuels, Europhysics News 47 (2016) 22-26.

[4] A. Navarrete, G. Centi, A. Bogaerts, Á. Martín, A. York, and G.D. Stefanidis, Harvesting Renewable Energy for Carbon Dioxide Catalysis, Energy Technology 5 (2017) 796–811.

[5] R. Snoeckx and A. Bogaerts, Plasma technology – a novel solution for CO_2 conversion?, Chem Soc. Rev (under revision) (2017)

[6] S.L. Suib, S.L. Brock, M. Marquez, J. Luo, H. Matsumoto, and Y. Hayashi, Efficient Catalytic Plasma Activation of CO_2, NO, and H_2O, Journal 102 (1998) 9661-9666.

[7] S. Paulussen, B. Verheyde, X. Tu, C. De Bie, T. Marterns, D. Petrovic*, et al.*, Conversion of carbon dioxide to value-added chemicals in atmospheric pressure dielectric barrier discharges, Plasma Sources Science and Technology 19 (2010) 034015.

[8] S. Kim, M. Lim, and Y. Chun, Reduction Characteristics of Carbon Dioxide Using a Plasmatron, Plasma Chemistry and Plasma Processing 34 (2014) 125-143.
[9] S.C. Kim and Y.N. Chun, Development of a gliding arc plasma reactor for CO_2 destruction, Environmental Technology 35 (2014) 2940-2946.
[10] A. Bogaerts, T. Kozák, K. van Laer, and R. Snoeckx, Plasma-based conversion of CO_2: current status and future challenges, Faraday Discussions 183 (2015) 217-232.
[11] D. Mei, X. Zhu, Y.-L. He, J.D. Yan, and X. Tu, Plasma-assisted conversion of CO_2 in a dielectric barrier discharge reactor: understanding the effect of packing materials, Plasma Sources Science and Technology 24 (2015) 015011.
[12] K. Van Laer and A. Boagaerts, Improving the converson and energy efficiency of CO_2 splitting in a ZrO_2 packed bed DBD reactor, Energy Technol 3 (2015) 1038-1044.
[13] R. Aerts, W. Somers, and A. Bogaerts, Carbon Dioxide Splitting in a Dielectric Barrier Discharge Plasma: A Combined Experimental and Computational Study, ChemSusChem 8 (2015) 702-716.
[14] A. Ozkan, A. Bogaerts, and F. Reniers, Routes to increase the conversion and the energy efficiency in the splitting of CO 2 by a dielectric barrier discharge, Journal of Physics D: Applied Physics 50 (2017) 084004.
[15] M. Ramakers, G. Trenchev, S. Heijkers, W. Wang, and A. Bogaerts, Gliding Arc Plasmatron: providing an alternative method for carbon dioxide conversion, ChemSusChem (2017) (in press).
[16] K. Zhang, G. Zhang, X. Liu, A.N. Phan, and K. Luo, A Study on CO_2 Decomposition to CO and O_2 by the Combination of Catalysis and Dielectric-Barrier Discharges at Low Temperatures and Ambient Pressure, Industrial & Engineering Chemistry Research 56 (2017) 3204-3216.
[17] T. Kozák and A. Bogaerts, Splitting of CO_2 by vibrational excitation in non-equilibrium plasmas: a reaction kinetics model, Plasma Sources Science and Technology 23 (2014) 045004.
[18] T. Kozák and A. Bogaerts, Evaluation of the energy efficiency of CO_2 conversion in microwave discharges using a reaction kinetics model, Plasma Sources Science and Technology 24 (2015) 015024.
[19] A. Berthelot and A. Bogaerts, Modeling of CO_2 Splitting in a Microwave Plasma: How to Improve the Conversion and Energy Efficiency?, J. Phys. Chem. C 121 (2017) 8236–8251.
[20] A. Fridman, Plasma Chemistry, Cambridge University Press, New York, 2008.
[21] J.F. de la Fuente, A.A. Kiss, M.T. Radoiu, and G.D. Stefanidis, Microwave plasma emerging technologies for chemical processes, Journal of Chemical Technology & Biotechnology (2017)
[22] V.D. Rusanov, A. Fridman, and G.V. Sholin, The physics of a chemically active plasma with nonequilibrium vibrational excitation of molecules, Soviet Physics Uspekhi 24 (1981) 447.
[23] W. Bongers, H. Bouwmeester, B. Wolf, F. Peeters, S. Welzel, D. van den Bekerom*, et al.*, Plasma-driven dissociation of CO_2 for fuel synthesis, Plasma Processes and Polymers 14 (2016) 201600126.
[24] G. Chen, T. Silva, V. Georgieva, T. Godfroid, N. Britun, R. Snyders*, et al.*, Simultaneous dissociation of CO_2 and H_2O to syngas in a surface-wave microwave discharge, International Journal of Hydrogen Energy 40 (2015) 3789-3796.
[25] G. Chen, V. Georgieva, T. Godfroid, R. Snyders, and M.-P. Delplancke-Ogletree, Plasma assisted catalytic decomposition of CO_2, Applied Catalysis B: Environmental 190 (2016) 115-124.
[26] G. Chen, N. Britun, T. Godfroid, V. Georgieva, R. Snyders, and M.-P. Delplancke-Ogletree, An overview of CO_2 conversion in a microwave discharge: the role of plasma-catalysis, Journal of Physics D: Applied Physics 50 (2017) 084001.
[27] H.S. Uhm, H.S. Kwak, and Y.C. Hong, Carbon dioxide elimination and regeneration of resources in a microwave plasma torch, Environmental Pollution 211 (2016) 191-197.
[28] C.M. Mitsingas, R. Rajasegar, S. Hammack, H. Do, and T. Lee, High Energy Efficiency Plasma Conversion of CO_2 at Atmospheric Pressure Using a Direct-Coupled Microwave Plasma System, IEEE Transactions on Plasma Science 44 (2016) 651-656.

[29] T. Silva, N. Britun, T. Godfroid, and R. Snyders, Study of CO_2 Decomposition in Microwave Discharges by Optical Diagnostic Methods, InTech (2016)
[30] T. Silva, N. Britun, T. Godfroid, J.v.d. Mullen, and R. Snyders, Study of Ar and Ar-CO_2 microwave surfaguide discharges by optical spectroscopy, Journal of Applied Physics 119 (2016) 173302.
[31] S. Heijkers, R. Snoeckx, T. Kozák, T. Silva, T. Godfroid, N. Britun*, et al.*, CO_2 Conversion in a Microwave Plasma Reactor in the Presence of N_2: Elucidating the Role of Vibrational Levels, The Journal of Physical Chemistry C 119 (2015) 12815–12828.
[32] J.F. de la Fuente, S.H. Moreno, A.I. Stankiewicz, and G.D. Stefanidis, Reduction of CO_2 with hydrogen in a non-equilibrium microwave plasma reactor, International Journal of Hydrogen Energy 41 (2016) 21067-21077.
[33] J.F. de la Fuente, S.H. Moreno, A.I. Stankiewicz, and G.D. Stefanidis, On the improvement of chemical conversion in a surface-wave microwave plasma reactor for CO_2 reduction with hydrogen (The Reverse Water-Gas Shift reaction), International Journal of Hydrogen Energy (2017)
[34] H.S. Kwak, H.S. Uhm, Y.C. Hong, and E.H. Choi, Disintegration of Carbon Dioxide Molecules in a Microwave Plasma Torch, Sci Rep 5 (2015) 18436.
[35] N. den Harder, D.C.M. van den Bekerom, R.S. Al, M.F. Graswinckel, J.M. Palomares, F.J.J. Peeters*, et al.*, Homogeneous CO_2 conversion by microwave plasma: Wave propagation and diagnostics, Plasma Processes and Polymers (2016) e1600120.
[36] T. Silva, N. Britun, T. Godfroid, and R. Snyders, Optical characterization of a microwave pulsed discharge used for dissociation of CO_2, Plasma Sources Science and Technology 23 (2014) 025009.
[37] R. Spitzl, B. Aschermann, and M. Walter Microwave plasma generator with the short cross-sectional side of the resonator parallel to the chamber axis *Google Patents* (2001)
[38] R. Snoeckx, Y.X. Zeng, X. Tu, and A. Bogaerts, Plasma-based dry reforming: improving the conversion and energy efficiency in a dielectric barrier discharge, RSC Advances 5 (2015) 29799-29808.
[39] N. Pinhão, A. Moura, J.B. Branco, and J. Neves, Influence of gas expansion on process parameters in non-thermal plasma plug-flow reactors: A study applied to dry reforming of methane, International Journal of Hydrogen Energy 41 (2016) 9245-9255.
[40] Comsol 5.0, CFD User's Guide.
[41] D. Wilcox, Turbulence Modeling for CFD DCW Industries Inc., La Cañada Flintridge, CA, 2006.
[42] W.M. Kays, Turbulent Prandtl Number—Where Are We?, Journal of Heat Transfer 116 (1994) 284-295.
[43] G. Gronald and J.J. Derksen, Simulating turbulent swirling flow in a gas cyclone: A comparison of various modeling approaches, Powder Technology 205 (2011) 160-171.
[44] L.F. Spencer and A.D. Gallimore, CO_2 dissociation in an atmospheric pressure plasma/catalyst system: a study of efficiency, Plasma Sources Science and Technology 22 (2013) 015019.
[45] L.F. Spencer and A.D. Gallimore, Efficiency of CO_2 Dissociation in a Radio-Frequency Discharge, Plasma Chemistry and Plasma Processing 31 (2011) 79-89.
[46] G. Trenchev, S. Kolev, W. Wang, M. Ramakers, and A. Bogaerts, CO2 conversion in a gliding arc plasmatron: Multidimensional modelling for improved efficiency, Journal of CO2 Utilization (2017)
[47] S.M. Chun, D.H. Choi, J.B. Park, and Y.C. Hong, Optical and Structural Properties of ZnO Nanoparticles Synthesized by CO2 Microwave Plasma at Atmospheric Pressure, Journal of Nanoparticles 2014 (2014) 7.
[48] A. Bogaerts, A. Berthelot, S. Heijkers, S. Kolev, R. Snoeckx, S. Sun*, et al.*, CO_2 conversion by plasma technology: Insights from modeling the plasma chemistry and plasma reactor design, Plasma Sources Science and Technology 26 (2017) 063001.

[49] G.J. van Rooij, D.C.M. van den Bekerom, N. den Harder, T. Minea, G. Berden, W.A. Bongers*, et al.*, Taming microwave plasma to beat thermodynamics in CO_2 dissociation, Faraday Discussions 183 (2015) 233-248.

[50] S. Mori, N. Matsuura, L.L. Tun, and M. Suzuki, Direct Synthesis of Carbon Nanotubes from Only CO2 by a Hybrid Reactor of Dielectric Barrier Discharge and Solid Oxide Electrolyser Cell, Plasma Chemistry and Plasma Processing 36 (2015) 231-239.

[51] S. Mori and L.L. Tun, Synergistic CO_2 conversion by hybridization of dielectric barrier discharge and solid oxide electrolyser cell, Plasma Processes and Polymers 14 (2016) e1600153.